Infection, Genetics and Evolution 83 (2020) 104321

Contents lists available at ScienceDirect

Infection, Genetics and Evolution

journal homepage: www.elsevier.com/locate/meegid

Research Paper

The complete genome sequence of bearded dragon adenovirus 1 harbors three genes encoding proteins of the C-type lectin-like domain superfamily

Judit J. Pénzes[a,b,*,1], Leonóra Szirovicza[a,2], Balázs Harrach[a]

[a] Institute for Veterinary Medical Research, Centre for Agricultural Research, Budapest, Hungary
[b] INRS-Institut Armand-Frappier Research Centre, Laval, Quebec, Canada

ARTICLE INFO

Keywords:
Adenoviridae
Atadenovirus
Bearded dragon
Genome organization
CTLD superfamily
Lectin

ABSTRACT

Bearded dragon adenovirus 1 (BDAdV-1), also known as agamid adenovirus 1, has been described worldwide as a prevalent infectious agent of the inland bearded dragon (*Pogona vitticeps*), the most common squamate exotic pet reptile. Previous limited sequence data of the adenoviral DNA polymerase and hexon genes indicated that BDAdV-1 is a member of genus *Atadenovirus* family *Adenoviridae*. Atadenoviruses infect ruminants, marsupials, testudine reptiles and birds, yet the genus has been shown to be of squamate reptile origin. Here, we report a screening survey along with the complete genome sequence of BDAdV-1, derived directly from the sample of a deceased juvenile dragon showing central nervous system signs prior to passing. The BDAdV-1 genome is 35,276 bp and contains 32 putative genes. Its genome organization is characteristic of the members of genus *Atadenovirus*, however, a divergent LH3 gene indicates structural interactions of different nature compared to other genus members such as snake adenovirus 1. We identified five novel open reading frames (ORFs), three of which encode proteins of the C-type lectin-like domain (CTLD) superfamily. ORF3 has a CTLD group II-like domain architecture displaying structural similarity with natural killer cell surface receptors and with an alphaherpesviral virulence factor gene for neurotropism, UL45. ORF4 and 6 are extremely long compared to typical adenoviral right-end genes and possibly encode members of the CTLD superfamily with novel, previously undescribed domain architectures. BDAdV-1 is the hitherto most divergent member of genus *Atadenovirus* providing new insights on adenoviral diversity, evolution and pathogenesis.

1. Introduction

Adenoviruses (AdVs) are medium sized, non-enveloped viruses having linear, dsDNA genomes (Harrach et al., 2011). AdVs were reported from almost all known classes of vertebrates: ray-finned fish, amphibians, reptiles, birds and mammals (Harrach et al., 2011; Harrach et al., 2019; Doszpoly et al., 2019; Davison et al., 2000; Farkas et al., 2008; Kaján et al., 2012; Vidovszky et al., 2019). AdVs (family *Adenoviridae*) are classified into five genera from which the members of genus *Atadenovirus* have a diverse range of hosts (Harrach et al., 2011; Harrach et al., 2019). Atadenoviruses have been detected in scaled reptiles (order Squamata; lizards, snakes, worm lizards) (Benkő et al., 2002; Wellehan et al., 2004; Abbas et al., 2011; Ball et al., 2014; Szirovicza et al., 2016; Prado-Irwin et al., 2018), birds (Harrach et al., 1997; Hess et al., 1997; To et al., 2014; Duarte et al., 2019; Needle et al., 2019; de Oliveira et al., 2020), ruminants (Harrach et al., 1997; Vrati et al., 1996; Fox et al., 2017; Miller et al., 2017), marsupials (Thomson et al., 2002; Gal et al., 2017), and a common tortoise (Garcia-Morante et al., 2016). The first detection of an adenovirus from bearded dragon (*Pogona vitticeps*) was accomplished from pet animals in the U.S.A. (Wellehan et al., 2004). This bearded dragon adenovirus 1 (BDAdV-1) was named also agamid adenovirus 1. Apparently the same virus type was detected also in Austria, Germany and Australia (Kübber-Heiss et al., 2006; Schilliger et al., 2016; Papp et al., 2009; Kubiak, 2013; Doneley et al., 2014). However, these and further studies detected genotype differences among the AdVs infecting the bearded dragons raised by hobby terraristic enthusiasts in the USA, Austria, Germany, UK and Australia (Wellehan et al., 2004; Kübber-Heiss et al., 2006; Papp et al., 2009; Schilliger et al., 2016; Kubiak, 2013; Doneley et al., 2014; Parkin et al., 2009). This virus seems to occur also in

* Corresponding author at: Institute for Veterinary Medical Research, Centre for Agricultural Research, Budapest, Hungary.
E-mail address: judit.penzes@ufl.edu (J.J. Pénzes).
[1] Present address: Department of Biochemistry and Molecular Biology, Center for Structural Biology, The McKnight Brain Institute, University of Florida, Gainesville, FL 32610, USA.
[2] Present address: Department of Virology, Faculty of Medicine, Medicum, University of Helsinki, Helsinki, Finland.

https://doi.org/10.1016/j.meegid.2020.104321
Received 6 March 2020; Received in revised form 9 April 2020; Accepted 10 April 2020
Available online 14 April 2020

central netted dragons (*Ctenophorus nuchalis*) in Australia (Hyndman and Shilton, 2011). The newest findings proved agamid AdV-1 to occur also in free-ranging Australian bearded dragons and a rather similar AdV was identified in coastal bearded dragon (*P. barbata*) (Hyndman et al., 2019). To date, BDAdV-1 remains a major concern of exotic veterinary science and the importance of its recognition and elimination from captive *P. vitticeps* breeding populations has been targeted throughout the United States (Fredholm et al., 2015). Although its pathogenesis is little understood, BDAdV-1 has been linked to various clinical signs, including sudden death, lethargy, weakness, diarrhoea, dehydration and anorexia. It has been proposed that BDAdV-1 may be responsible for central nervous system signs observed in young dragons, namely paresis, head tilt, circling, and opisthotonos, due to its pathology in the liver (Wellehan et al., 2004, Kübber-Heiss et al., 2006, Papp et al., 2009, Parkin et al., 2009, Doneley et al., 2014, Schilliger et al., 2016,). However, subclinical BDAdV-1 infection has also been described (Kubiak, 2013).

Members of the *Adenoviridae* family have been widely characterized as far as their genome content is concerned. Their linear genome, ranging from 25 to 48 kb in size, encodes proteins on both strands, transcribed either in a rightward (*r*) or a leftward (*l*) orientation. At the genome termini, inverted terminal repeats (ITRs) of various length are present (Harrach et al., 2011). Comparative analyses indicate that all AdV genomes possess a highly-conserved set of genes comprising the central region of their genomes. These genes are present throughout the entire family and encode proteins of either structural or fundamental replication function (Davison et al., 2003; Harrach et al., 2011). As a general rule, genus specific genes are located toward the genome termini, followed by genes of even less conservation. The right end of adenoviruses of almost each adenoviral species thus far has been shown to be unique and highly varied throughout the family. In case of genus *Atadenovirus*, this is comprised by the genes located rightward from the E4 region, namely the RH region and open reading frames (ORFs) in a proximity of the right termini (Vrati et al., 1996; Hess et al., 1997; Dan et al., 2001; Farkas et al., 2008; To et al., 2014; Pénzes et al., 2014; Miller et al., 2017). Some of the type-specific and genus-specific AdV genes have been shown to harbour homology or similar domain architecture with genes of non-adenoviral origin, suspected to have been co-opted from members of distant virus families or from their hosts (Chiocca et al., 1996; Kaján et al., 2012; Doszpoly et al., 2019).

The C-type lectin-like domain (CTLD) superfamily is a large group of extracellular, mostly carbohydrate-binding proteins present in every major metazoan lineage (Zelensky and Gready, 2005). Members of the superfamily, known as CTLD containing proteins (CTLDcps) are classified into twelve groups based on their domain architecture and associated function. Group II and group V members harbour similar domain architecture and encompass asialoglycoproteins and natural killer (NK) cell surface receptors, respectively (Stockert, 1995; Middleton et al., 2002). Interestingly, viruses of multiple, distant lineages have been detected to harbour CTLDcp-encoding genes or even to express these as structural proteins, including *Poxviridae*, *Asfarviridae*, *Herpesviridae* and genus *Aviadenovirus* of *Adenoviridae* (Chiocca et al., 1996; Ensser et al., 1997; Wilcock et al., 1999; Afonso et al., 2000; Galindo et al., 2000; Mullen et al., 2002). All viral CTLDcps been found to display a group II/V-like domain architecture i.e. a short cytoplasmic tail followed by a transmembrane domain, a short stalk region and a single CTLD.

Here, we report the complete genome sequence of BDAdV-1 and confirm its affiliation with genus *Atadenovirus* of *Adenoviridae*. Furthermore, we show that BDAdV-1 possesses the longest atadenoviral genome thus far and harbors a unique genome organization. This is demonstrated by the presence of five type-specific genes, which lack any direct homology to any known adenoviral genes. Three of these are potential members of the CTLD superfamily and are of possible host origin. Two of these appear to harbour unique domain architectures, which cannot be assigned to any of the currently established CTLD superfamily groups. Lastly, we describe the results of a screening survey, conducted in Hungary, which, in concordance with our in silico analyses, may indicate BDAdV-1 to be a neurotropic infectious agent of juvenile inland bearded dragons.

2. Materials and methods

2.1. Samples

All samples involved in this study originated from bearded dragons deceased at Hungarian pet stores or were provided by private persons as carcasses. As the animals were captive-bred and kept, their previous history of clinical signs could be well-documented. Upon their arrival at our laboratory, each carcass was individually assessed for pathological signs and subjected to necropsy in a sterilized environment using sterile equipment in the process. Internal organs were collected, pooled, and subjected to DNA isolation.

2.2. DNA isolation and PCR screening

For nucleic acid extraction, 1 ml of 1 × TE buffer (10 mM Tris-HCl, 1 mM EDTA, pH 8.0) was added to the organs, previously placed into 2 ml microcentrifuge tubes. Following sample homogenization by a Qiagen Tissue Lyser II (Qiagen), DNA was purified from 100 µl homogenate. Briefly, we added 4 µl proteinase-K (20 mg/ml) and 10 µl sarcosyl (10%) solution to the mixture, which we subjected to overnight digestion in a thermomixer at 55 °C. The next day 300 µl guanidine-hydrochloride (8 M) and 20 µl ammonium-acetate solution (7.5 M) was added. The mixture was incubated for one hour with gentle mixing in every 15 min. The nucleic acids were precipitated by adding absolute ethanol (− 20 °C). After centrifugation, the pellet was washed with 70% ice-cold ethanol. After the evaporation of ethanol, the DNA was re-suspended in 50 µl of nuclease-free water.

To check the presence of adenoviral DNA, a sensitive consensus nested PCR, targeting a highly conserved region of the adenoviral DNA-dependent DNA polymerase gene, was employed (Wellehan et al., 2004). The amplification product, following the second amplification step, was an approximately 320-bp-long fragment. The PCRs were performed in 50 µl final volume, using either the REDTaq® ReadyMix™ (Sigma-Aldrich®) or the DreamTaq™ (Thermo Fisher®) DNA polymerase enzyme according to the manufacturers' recommendation. The thermal profile of the PCR was identical to the originally described (Wellehan et al., 2004) except for the denaturation steps set at 95 °C.

2.3. Complete genome sequencing

In our laboratory, we designed multiple sets of primers to amplify short, conserved regions by PCR from the p32K, IVa2, penton, pVII, hexon and 100 K genes. The sequence of all sets of consensus oligos, as well as their annealing temperature and expected target size are summarized by table S1. All PCR amplifications were performed in a reaction volume of 50 µl using a program of an initial denaturation step at 95 °C for 5 min, followed by 45 cycles of denaturation at 95 °C for 30 s and annealing at a temperature five degrees lower than the predicted melting temperature (Tm) of the primer set used, for 1 min. The elongation step took place at 72 °C for 1 min, followed by final elongation at 72 °C for 5 min. To amplify a 900-bp-long fragment encompassing the partial penton base and pVI, but complete pVII and pX genes, we utilized the PCR system previously described by Szirovicza et al. (2016).

The PCR products were purified and sequenced directly on both strands. We performed the sequencing reactions using the BigDye® Terminator v3.1 Cycle Sequencing Kit (Life Technologies Corporation®), and sent them for electrophoresis by a commercial service at Baygen Institute (Szeged, Hungary) on an ABI PRISM 3100 Genetic Analyzer (Life Technologies Corporation).

To fill in the gaps between the short fragments amplified by the

consensus oligos, we utilized the Phusion High-Fidelity DNA Polymerase™ (Thermo Fisher Scientific®) with the reaction conditions described above, but changing the elongation time to correspond with the length of the expected product, using 1 kb/min as a general rule. The amplified fragments were blunt-end cloned into either the pre-cut pCRTM-Blunt II-TOPO® vector (Thermo Fisher Scientific), conjugated with terminal topoisomerase, or into the pJet 1.2/blunt vector (Thermo Fisher Scientific). Ligation took place at room temperature for 30 min, or at 4 °C overnight in case of inserts larger than 5 kb. Sequencing of the insert took place as described above. To amplify extensive regions with little to no conservation, such as the right end of the genome, we designed single primer PCRs with longer annealing time of 2 min, annealing temperature of 50 °C and elongation time of 5 min, to the rightmost known sequence at the time of the genome. The amplified product was also cloned and sequenced.

2.4. Sequencing of the genome termini

The adenoviral ITRs are notoriously difficult to clone, due to the associated terminal protein (TP). To overcome this, a specific leftward primer was designed from the sequence of the putative p32K gene. After DNA denaturation a polyA tail was added to the 3′ end of the genome using terminal transferase from the 5′/3′ 2nd Generation RACE Kit 190 (Roche Applied Science). By utilizing the above-mentioned p32K-specific primer together with a polyT anchor primer, the region could be amplified and sequenced. There was no annealing time incorporated into the PCR program used.

2.5. In silico analyses

The sequence of the PCR-amplified fragments as well as the sequences consequently obtained by primer walking, were subjected to homology search in the NCBI GenBank databases, using the Blast algorithms. For identification and comparison of the obtained nucleotide sequences, Blastn was applied to determine nucleotide-level homology and we used Blastx to determine whether the obtained sequence is from a coding region and if so, from which exact adenoviral gene. Sequence editing and assembly was performed by applying the Staden Sequence Analysis Package (Staden et al., 2000). The genome annotation was carried out using Artemis Genome Browser (Carver et al., 2012). Potential splice acceptor and donor sites were examined manually as well as using the NNSPLICE 0.9 application (Reese et al., 1997). The derived protein sequence of each ORF was searched by multiple applications to identify conserved domains or motifs. TM domains were detected using the TMHMM package v.2.0 (Krogh et al., 2001) and we used SignalP v.5.0 (Almagro Armenteros et al., 2019) to identify possible signal peptides. To find domains of known homology and to investigate protein domain architecture, we used SMART (Letunic and Bork, 2018).

To assess structural similarity of the derived protein sequences to protein structures deposited to PDB, we used the pGenThreader algorithm of the PSIPRED workbench (Lobley et al., 2009). To identify individual domains and to predict their structural similarity to any known characteristic fold, we used the pDomThreader algorithm (Lobley et al., 2009). To construct homology models we used Swiss Model (Waterhouse et al., 2018), incorporating the pGenThreader results as templates for the modelling. Individual domains were folded by Modeller v9.23 (Webb and Sali, 2016), incorporating the results of pDomThreader. Homology models were viewed and illustrated by UCSF Chimera (Pettersen et al., 2004).

2.6. Phylogenetic calculations

We collected the homologous protein sequences from the NCBI databases and used them to construct multiple sequence alignments with the M-Coffee algorithm of T-Coffee (Wallace et al., 2006). The alignments were viewed and edited using Unipro UGENE v1.18 (Okonechnikov et al., 2012). For each protein, a guide tree was constructed using the ProtDist and Fitch programs of Phylip v3.698, with a Jones-Taylor-Thornton matrix, incorporating global rearrangements (Felsenstein, 1993). Model selection was carried out by ProtTest v2.4 (Darriba et al., 2011) and the suitable substitution model was determined based on the Akaike and Bayes information criteria. The model used for the pol and penton base calculations were LG + I + G + F, with α of 0.727 and 0.819, respectively along with pInv of 0.121 and 0.181, respectively. In case of the pVII calculations, we used the VT + I + G + F model with an α of 1.408 and pInv of 0.059. We performed the maximum likelihood analysis using the PhyML v3.1 incorporating the parameters established by the aforementioned model selection (Guindon et al., 2010). The reliability of tree topology was tested by performing bootstrap analysis in case of the pol and penton base calculations. Due to its size (124 aa) and the alternating nature of highly-conserved and highly variable regions, we tested the topology with aLRT-Shimodaira-Hasegawa-like test, to avoid unreliable distortion caused by random weights. Phylogenetic trees were visualized using the FigTree v1.4.2. software of the BEAST package (Suchard et al., 2018).

3. Results

3.1. Screening survey of bearded dragon samples

Between the years 2009 and 2017, the samples of 28 deceased inland bearded dragons were PCR-screened by a consensus nested PCR system targeting an approx. 300-bp-long segment of the adenoviral DNA-dependent DNA polymerase gene (pol) (Wellehan et al., 2004). The screened samples included pulled organs of the dragons, notably the liver, spleen, lungs, gonads and kidneys. All dragons originated from local pet stores. Out of the 26 samples, found to be positive for the AdV presence, twelve originated from juvenile dragons of one to four months of age, showing sever central nervous system (CNS) signs prior to their passing. Eight more adults and two juvenile animals showed signs of anorexia, disecdysis, an increased volume of fluids in their abdominal cavity, with some of them having difficulties of lifting their cloaca from the ground. The remaining positive animals, namely four adults and two juveniles, displayed no noticeable signs before passing. The 30 pol sequences obtained from the positive samples showed slight variations at nucleotide level, hence four genotypes could be distinguished (Fig. 1a). Since the pol has been shown to be one of the most conserved genes of the AdV genome, the short pol sequences were designated as separate genotypes if they were differing in at least one nucleotide from each other (Wellehan et al., 2004; Parkin et al., 2009; Harrach et al., 2011). Genotypes identified in this study were labelled as 'H' after Hungary being the geographic location of their identification and supplied with a number to differentiate them. Two of these, referred to as H1 and H2, are previously undescribed ones and each have been derived from only one juvenile dragon, respectively. Genotype H3, which had previously been detected in Austria, Germany, the United States and Australia was present in the samples of 20 dragons (Kübber-Heiss et al., 2006; Parkin et al., 2009; Papp et al., 2009; Hyndman and Shilton, 2011). Genotype H4, previously described to occur in the United States, was derived from eight samples, of which two also harboured H3 and one was simultaneously infected by H1 and H3 as well. Once the sequencing and annotation of the complete BDAdV-1 genome was completed, the PCR testing of the brain tissue of six dragons was carried out additionally. Three juveniles with prior CNS signs tested positive, while an adult and juvenile with prior signs but lacking the CNS ones, along with another adult with no prior signs tested negative (Fig. 1b). Then results of the screening survey are summarized in Table 1.

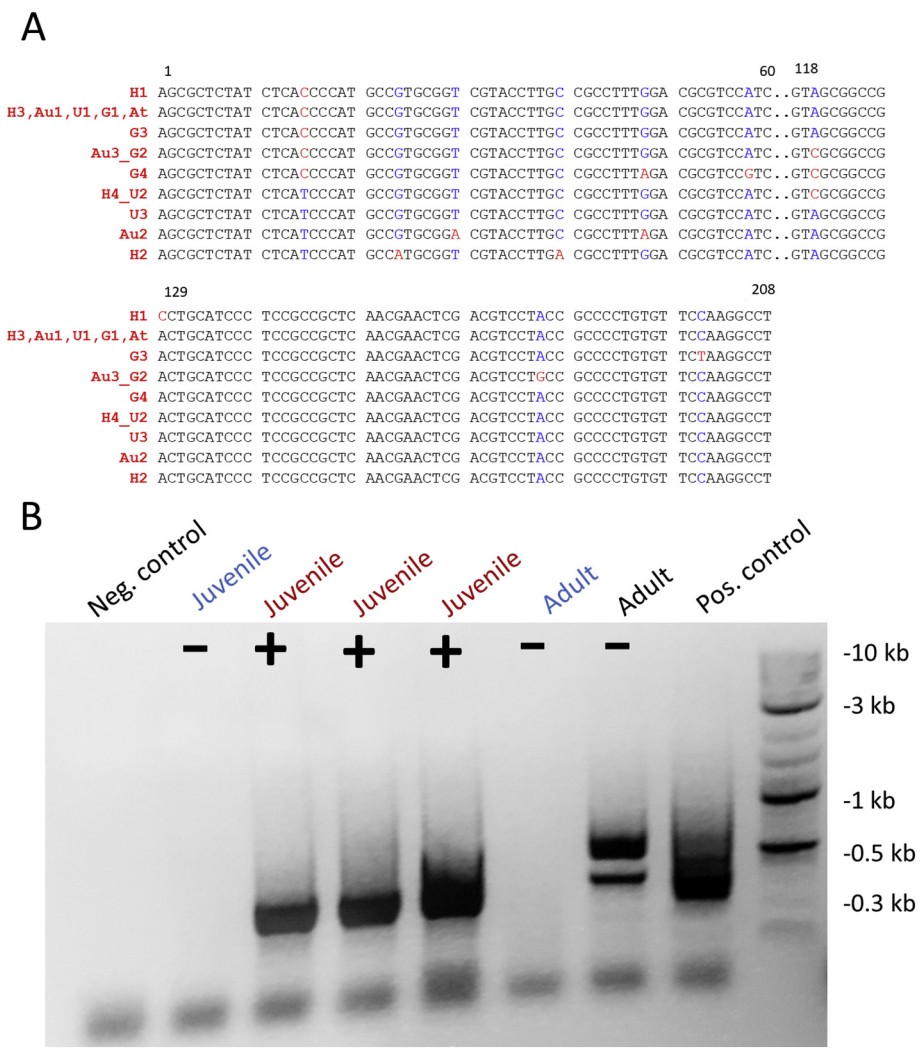

Fig. 1. Investigation of bearded dragon adenovirus 1 prevalence and nucleotide level diversity. Panel A presents an alignment of all four genotypes detected in Hungary, during this study, marked as "H", aligned with all hitherto detected genotypes around the world. Country affiliations are indicated as follows: At – Austria, Au – Australia, G – Germany, U – United States. Panel B displays the results of DNA-dependent DNA polymerase-based consensus PCR screening of the brain tissue derived from samples previously proven positive for bearded dragon adenovirus 1 DNA presence in internal organs. Samples indicated with red demonstrated central nervous system signs prior to passing, blue ones presented a variety of signs with the exception of central nervous system ones, whereas black ones had no recognizable clinical history. Lizard adenovirus 2 was applied as positive control. (For interpretation of the references to colour in this figure legend, the reader is referred to the web version of this article.)

3.2. The complete genome sequence of bearded dragon adenovirus 1

We managed to obtain the complete genome sequence of the H2 BDAdV-1 genotype directly from a juvenile *P. vitticeps* specimen demonstrating CNS signs prior to its passing. The complete BDAdV-1 genome has been deposited to GenBank under accession number MT050041. It included 35,276 base pairs (bp) of which 194 bp comprises the ITRs, with an average GC content of 56.21%. We identified 32 putative genes, of which 27 demonstrated homology with previously described adenoviral genes (Fig. 2).

The left end of the genome contained a homologue of p32K on the *l* strand. This was followed by three LH genes on the *r* strand, namely LH1, LH2 and LH3. Fold recognition by pGenThreader indicated the BDAdV-1 LH3 protein to display structural similarity with the snake adenovirus 1 (SnAdV-1) LH3 crystal structure (p = 7e-14, RCSB Protein Data Bank (PDB) ID: 5G5O) as well as with that of the tailspike attachment protein of *Escherichia coli* bacteriophage HK620 (species *Salmonella virus HK620*, p = 3e-07, PDB ID: 4XOT). We managed to build a homology model of the BDAdV-1 LH3, using the protein structure of the SnAdV-1 LH3 as a target (Menendez-Conejero et al., 2017). The model clearly displays the trimeric β spiral fold of bacteriophage tailspike attachment proteins and possibly forms a homotrimer, similarly to its SnAdV-1 homologue (Fig. 3). Superimposition of the BDAdV-1 LH3 homology model with the SnAdV-1 LH3 crystal structure model indicated that structural differences are limited only to the outer loops, despite of the low sequence identity of only 28.3%. When comparing the residues responsible for the interactions of the SnAdV-1 LH3 with the neighbouring hexon towers, only two (Arg175, Asp197) were identical (Menendez-Conejero et al., 2017). The sidechain charge, however, is maintained by two more residues (Asp107 vs. Glu109), whereas both Lys58 and Arg159 had been substituted with negatively-charged Thr residues instead (Fig. 3a).

At the centre of the BDAdV-1 genome the conserved E2 region was identified on the *l* strand, including the U-exon and DNA-binding protein (DBP) of E2A and three genes of the E2B, namely IVa2, pol and the precursor of the terminal protein (pTP). While the IVa2 DNA sequence did not indicate the presence of any canonical mRNA splice sites, we managed to identify a potential splice acceptor site (CTTCTTAG/A) and a small upstream leader of four amino acids (aa) with a donor site (AAG/GTAAG) for the pTP. The ORF encoding the polymerase gene did not display any canonical ATG start codons, with the first Met appearing only 219 aa downstream from the first residue of the frame. Downstream the fourth residue of the ORF, however, a canonical splice acceptor site sequence (CTCTCTCTTAG/G) was present, which appeared to be capable of putting the polymerase ORF in frame with the aforementioned pTP leader donor site, similarly to what has been described in members of genus *Mastadenovirus* (Davison et al., 2003; Zhao et al., 2014).

Homologues of all conservative adenoviral late genes were identified on the *r* strand, regulated by the major late promoter, namely the 52 K, pIIIa, penton base (III), pVII, pX, pVI, hexon (II), protease, 100 K, 22 K and pVIII. A potential splice donor site was identified in the 22 K

Table 1
The distribution of positive and negative samples.

Age group	Clinical signs	Genotypes detected	Results of brain tissue PCR
adult	Egg retention, inflamed ovaria	Negative	N/A
adult	None	Negative	N/A
Juvenile[c]	CNS[a], anorexia, dysecdysis	H2	positive
juvenile	CNS, anorexia	H3	positive
juvenile	CNS, anorexia, dysecdysis	H3	positive
juvenile	CNS	H3	N/A
juvenile	CNS, fluid-filled abdomen	H3, H4	N/A
juvenile	CNS, fluid-filled abdomen, anorexia	H3	N/A
juvenile	CNS, anorexia	H3, H4	N/A
juvenile	CNS, anorexia	H3	N/A
juvenile	CNS	H3	N/A
juvenile	CNS, MBD[b], anorexia	H3, H4, H1	N/A
juvenile	CNS, dysecdysis	H3	N/A
juvenile	CNS, anorexia	H3	N/A
juvenile	Fluid-filled abdomen; enlarged, fluid filled heart	H4	negative
juvenile	Anorexia, dysecdysis, missing claws, MBD, could not lift cloaca from ground	H3	N/A
juvenile	No visible clinical signs	H3	N/A
juvenile	No visible clinical signs	H3	N/A
juvenile	No visible clinical signs	H3	N/A
juvenile	No visible clinical signs	H4	N/A
adult	Egg retention, fluid-filled abdomen	H3	N/A
adult	Anorexia, dysecdysis, could not lift cloaca from ground	H4	N/A
adult	Anorexia, MBD, could not lift cloaca from ground	H3	N/A
adult	Anorexia, dysecdysis, could not lift cloaca from ground	H3	negative
adult	No visible clinical signs	H3	negative
adult	No visible clinical signs	H4	N/A
adult	No visible clinical signs	H4	N/A
adult	No visible clinical signs	H3	N/A

[a] CNS: Central nervous system signs.
[b] MBD: Metabolic bone disease.
[c] Complete genome sequence determined from this sample.

ORF (TC/GTAAG), which is potentially capable of putting the acceptor site of a small downstream exon in frame (TTCCTTTTTTCAG/G), possibly expressing the 33 K protein, similarly to all AdVs to date (Davison et al., 2003, Harrach et al. 2011, Zhao et al., 2014). Only one ORF demonstrated homology with AdV fiber genes. The BDAdV-1 derived fiber protein sequence displayed equally 30–32% aa identity with various mastadenoviral and atadenoviral fiber sequences. The C-terminal 142 residues were unrecognized by blastp searches, possibly corresponding with the knob region (Singh et al., 2014; Nguyen et al., 2015). The hydrophobic residue triplets, comprising the β strands stabilizing the β-spiral fold of the fiber shaft region of the BDAdV-1 fiber probably form twelve such spiral repeats. Although fold recognition by pGenThreader identified the β-spiral homotrimer repeats with a significant score (p = 5e-06), the assessed knob region could not be revealed to share structural similarity with any protein structures deposited to the PDB thus far.

3.3. The E4, RH and right end region of BDAdV-1

We compared the variable right end of the genome, past the fiber gene, with the corresponding region of all completely-sequenced atadenovirus genomes thus far, each classified as distinct species (Fig. 4). In BDAdV-1 three E4 genes located on the *l* strand. The RH region, which located directly rightward of the E4 genes, was composed of only one RH gene on the *l* strand, which potentially expresses a protein of 246 residues. In its derived aa sequence two F-box Pfam domains were identified, both in proximity of the N-terminus (Fig. 5). The RH gene was followed by a 416-bp-long sequence, which included several low complexity regions of extensive single nucleotide stretches and lacked potential coding ORFs.

The derived protein sequence of ORF1, being the first *r*-strand-located ORF rightward from the RH gene, demonstrated 39% aa identity with ORF1 of lizard adenovirus 2 (LAdV-2). However, 29.5 and 32% aa identity was also displayed with the ORF1 genes of psittacine adenovirus 3 (PsAdV-3) and duck adenovirus 1 (DAdV-1), respectively. The first sixteen residues were identified as a secretory signal (likelihood of 0.9985 as predicted by SingnalP), which was followed by a type 2-like AdV protease cleavage site (WVGG/A) (Harrach et al. 2003).

The following five ORFs did not demonstrate any significant sequence identity with any adenoviral proteins deposited to the GenBank thus far. ORF2 possibly encodes a small protein of 10.4 kDa of predicted molecular weight. Its deduced protein sequence contains an N-terminal transmembrane (TM) helix, which is followed by a domain demonstrating sequence similarity with the 11 kDa proteins of baculoviruses (*E*-value = 0.019, predicted by SMART) in its cytoplasmatic domain (Fig. 5).

The protein sequence of ORF3 demonstrated over 90% coverage and identity of 25–40% with various avian and reptilian C-type lectin NK cell surface receptors. Fold recognition by pGenThreader indicated significant structural similarity between the ORF3 protein sequence and the murine Lγ49L4 NK cell receptor crystal structure (p = 2e-05, PDB ID: 3G8K), hence we constructed a homology model using this PDB entry as template. Based on this, ORF3 harbors an N-terminal TM domain followed by a cytoplasmatic CTLD (Fig. 6a). The CTLD displayed all elements of the canonical fold characteristic of the CTLD superfamily, namely a double loop structure, linking two anti-parallel β sheets (β1 and β5, also complemented by an N-terminal β0 strand,

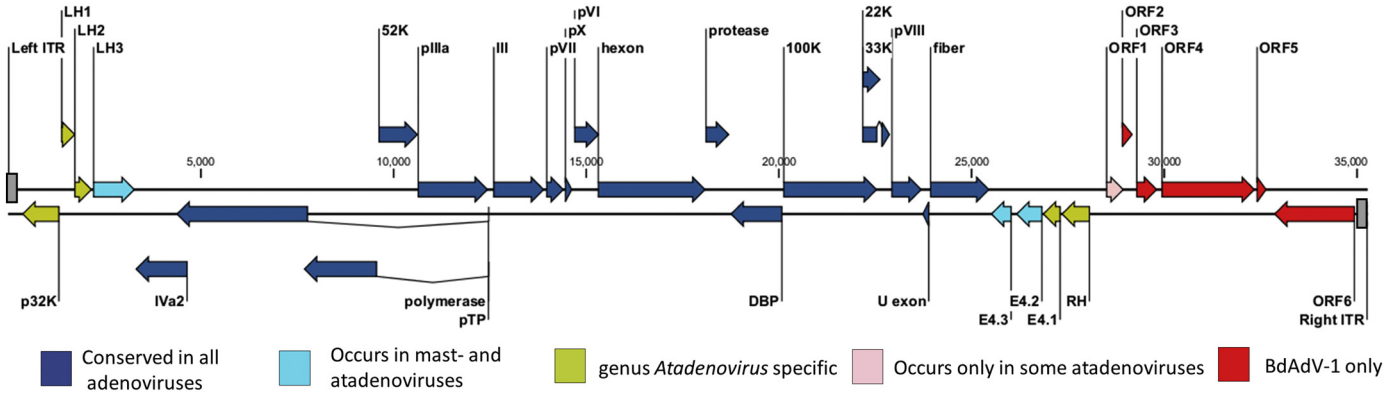

Fig. 2. Schematic map of the bearded dragon adenovirus 1 genome structure. The arrows symbolize genes and open reading frames (ORFs), indicating their direction of transcription. The conservation of each gene or ORF is colour coded, as indicated by the colour key in the legend.

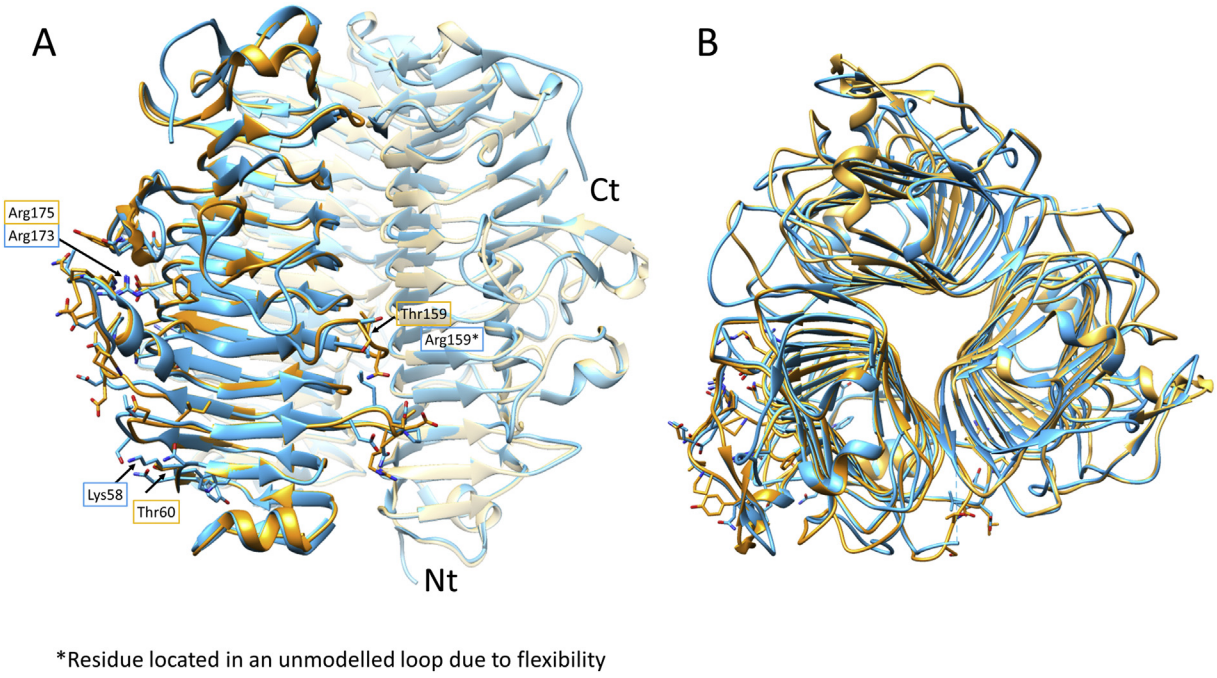

Fig. 3. Comparison by superimposition of the bearded dragon adenovirus 1 (BDAdV-1) LH3 homology model trimer with the crystal structure of the snake adenovirus 1 (SnAdV-1) LH3 protein. Panel A shows the trimer from a lateral view, with Nt and Ct indicating the N- and C-terminus of one of the monomers, respectively. Panel B shows the trimer from a top view. The yellow ribbon diagram corresponds with the BDAdV-1 LH3, whereas the crystal structure model backbone of the SnAdV-1 LH3 is demonstrated by the blue ribbon diagram. The atomic structure of amino acid sidechains of the corresponding colour indicates the residues shown to be responsible for the interaction of LH3 with the surrounding towers of the major capsid protein, the hexon. The three residues indicated by the arrows comprise the positively-charged patch, thought to be an important element of the structural interaction in case of the SnAdV-1 virion. The frames of the boxes, containing the residue names the arrows indicate, are presented in the corresponding colour to the model they refer to. (For interpretation of the references to colour in this figure legend, the reader is referred to the web version of this article.)

opposed to β2, β3, and β4) and flanked by two α helices (α1 and α2) (Zelensky and Gready, 2003). All four canonical Cys residues could be identified, forming two disulphide bridges, which stabilize the fold.

ORF4 is capable of expressing a large protein of 89.6 kDa, predicted to harbour an N-terminal TM domain followed by four cytoplasmatic CTLDs (Fig. 5). It demonstrates 20–25% sequence identity and no greater than 70% coverage with macrophage mannose receptors and macrophage mannose receptor-like CTLDcps of avian and fish origin. pGenThreader failed to detect possible structural similarity, which would span at least 70% of the protein sequence. By modelling the recognized domains separately, however, all four CTLDs could be folded, displaying the aforementioned canonical CTLD fold (Fig. 6b).

ORF5, the last potential protein-coding gene located on the *r* strand, is capable of encoding a small protein similar in size to ORF2 (10.4 kDa) (Fig. 5). Apart from identifying an N-terminal TM domain in its aa sequence, it demonstrated no significant similarity to any proteins described thus far.

ORF6 is the only potential gene of the region, which is located on the *l* strand. It is predicted to encode a large, multidomain protein of 78.1 kDa. Its deduced aa sequence included three potential CTLDs, followed by a C-terminal twisted gastrulation (Tsg) domain, with only low support, however (E-value = 6.8 as predicted by SMART). Blastp hits revealed aa sequence identity of 20–25% at coverage of 15–64% with CTLDcps of various groups, identified in mammalian, avian and fish vertebrates as well as in Nematoda invertebrates. Just like for ORF4, fold recognition was concluded to be unsuccessful in case of ORF6 as well. Homology models of all three CTLDs, nevertheless, could be constructed separately, to confirm the presence of the CTLD fold (Fig. 6c). All CTLDs identified in this study were supported with an E-value lower than 0.05, based on the SMART predictions.

3.4. Phylogeny inference

Maximum likelihood phylogenetic calculations based on a non-structural (pol) and two structural (penton, pVII) proteins unequivocally indicated BDAdV-1 to be a member of genus *Atadenovirus* (Fig. 7). The location of the BDAdV-1, however, varied greatly among the three separate reconstructions. The monophyly of reptilian atadenoviruses was only supported by the calculations based on the penton base, the only immunogenic protein out of the three represented here (Tischer et al., 2016). For purposes of reproducibility, all three alignments are shown as supplementary data (Figs. S1, S2 and S3).

4. Discussion

The complete genome sequence of BDAdV-1 is that of the ninth type of genus *Atadenovirus* yet only the third reptilian one. However, unlike the isolates of SnAdV-1 and LAdV-2, the BDAdV-1 genome was obtained directly from the sample of a deceased animal. Despite of being the longest member of the genus, it is only the second to LAdV-2 as far as the number of the potential protein encoding ORFs is concerned (Pénzes et al., 2014). When the SnAdV-1 genome analysis was completed, it was hypothesized that reptilian atadenoviruses, unlike their ruminant and avian counterparts, harbour shorter genomes and require less type specific genes in order to replicate efficiently (Farkas et al., 2008). The complete genome of BDAdV-1, similarly to the one of LAdV-2, contradicts to this (Pénzes et al., 2014).

The length of AdV ITRs varies significantly throughout the family, being over 100 bp in case of *Mastadenovirus*, *Ichtadenovirus* and most of *Aviadenovirus*, though shorter than 50 bp in *Siadenovirus* (Harrach et al. 2011, Doszpoly et al., 2019). The 194-bp-long ITRs of BDAdV-1, along with the ones of SnAdV-1 (118 bp) and LAdV-1 (126 bp) are in strong contrast with those of non-reptilian atadenoviruses (40–59 bp) (Hess

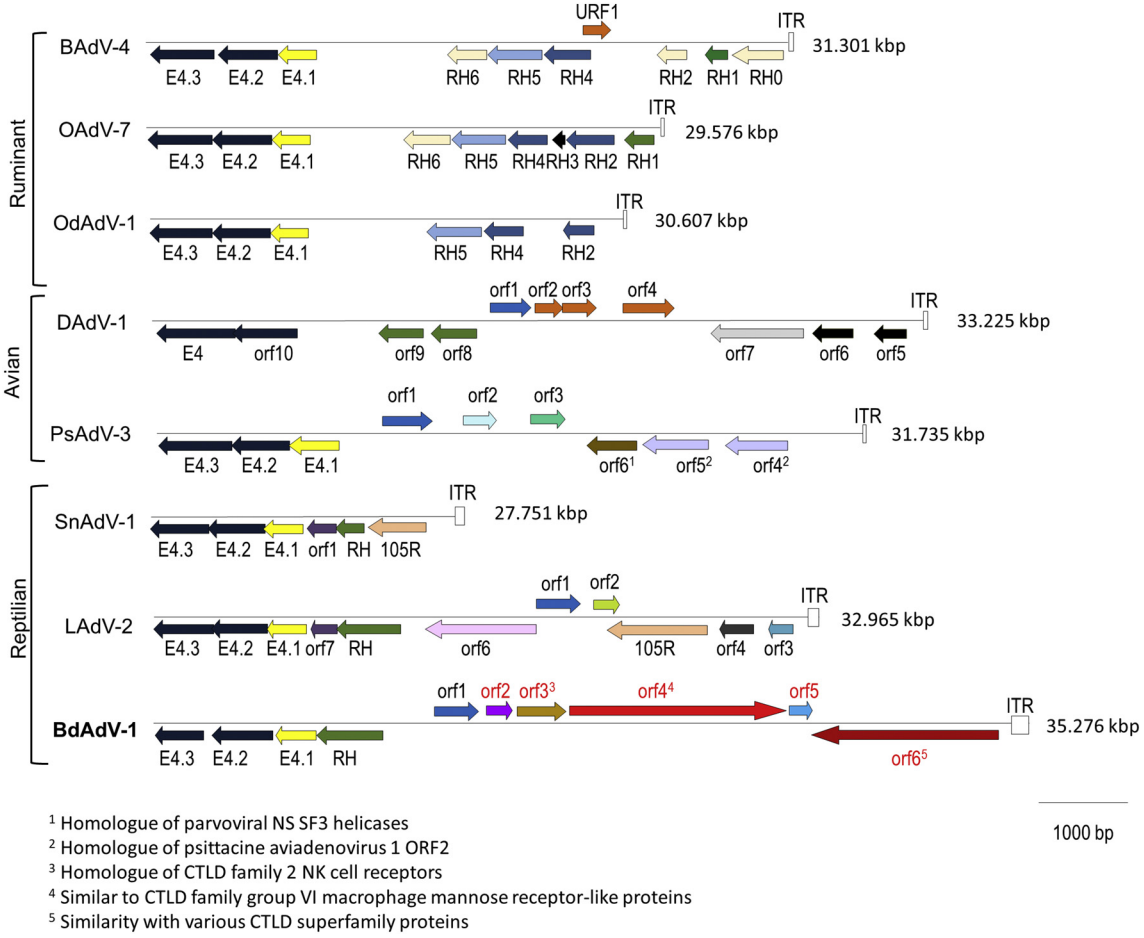

Fig. 4. Comparison of the variable right end region of members of genus *Atadenovirus*. The arrows indicate the size and direction of the open reading frames (ORFs) rightward of the fiber gene. ORFs demonstrating homology are shown in the same colour. The red letters indicate the five novel genes of bearded dragon adenovirus 1. (For interpretation of the references to colour in this figure legend, the reader is referred to the web version of this article.)

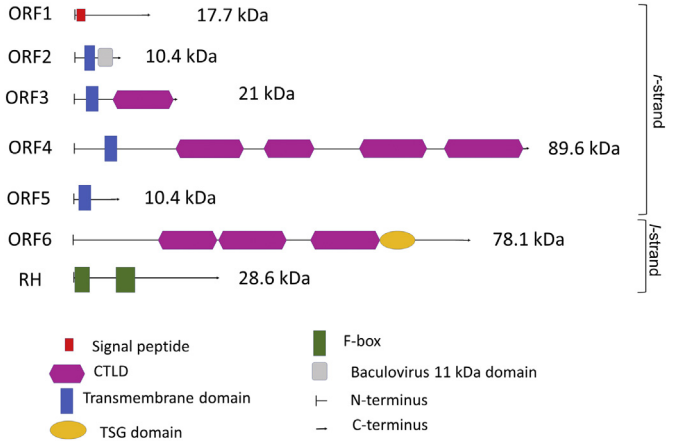

Fig. 5. Predicted domain architecture of the bearded dragon adenovirus 1 proteins expressed by the open reading frames (ORFs) located rightward from the E4 region.

et al., 1997, Vrati et al., 1996, Dan et al., 2001, Farkas et al.2008, Pénzes et al., 2014, To et al., 2014, Miller et al., 2017). As genus *Atadenovirus* is thought to be of squamate reptile origin, the shortening of the ITRs might be one the consequences of their adaptation to new hosts (Harrach et al., 1997; Wellehan et al., 2004; Farkas et al., 2008; Pénzes et al., 2014). This is in concordance with the shortness of *Siadenovirus* ITRs. Genus *Siadenovirus* is of mixed host affiliation with unknown host origin (Davison et al., 2000; Kovács and Benkő, 2011; Park et al., 2012). A similar tendency can be observed in the reduction of the overall genomic GC content, as both non-reptilian atadenoviruses and siadenoviruses generally harbour AT-rich genomes (Park et al., 2012; Kovács and Benkő, 2011; Davison et al., 2000; Miller et al., 2017; Hess et al., 1997; Vrati et al., 1996). Only psittacine AdV-3 is an exception, showing a balanced GC content of 53.54% (To et al., 2014). Both the SnAdV-1 and the LAdV-1 genomes possess balanced GC contents and this tendency is true even for short genome fragments derived from various squamate reptilian atadenoviruses (Wellehan et al., 2004; Farkas et al., 2008; Pénzes et al., 2014; Papp et al., 2009; Szirovicza et al., 2016; Ball et al., 2014; Prado-Irwin et al., 2018). The GC content of the BDAdV-1 (56.21%), though slightly higher than what could be considered balanced, still fulfils this tendency.

Host switch events have also been shown to increase AdV virulence (Garcia-Morante et al., 2016; Gal et al., 2017; Fox et al., 2017; Needle et al., 2019; Phalen et al., 2019). Our results indicate that BDAdV-1 is extremely prevalent in captive reptiles in Hungary. The presence of various genotypes and multiple subclinical cases could imply that BDAdV-1 has been adapting to the *P. vitticeps* for an extensive amount of time. This is in concordance with the worldwide identification of certain genotypes, such as H3 and H4, suggesting that dragons with no apparent signs get to be transported between breeders even intercontinentally, potentially infected by and hence carrying BDAdV-1. As our screening survey lacks the examinations aiming at the detection of additional infectious agents, it would be premature to conclude that any of the dragons died as a consequence of BDAdV-1 infection. The

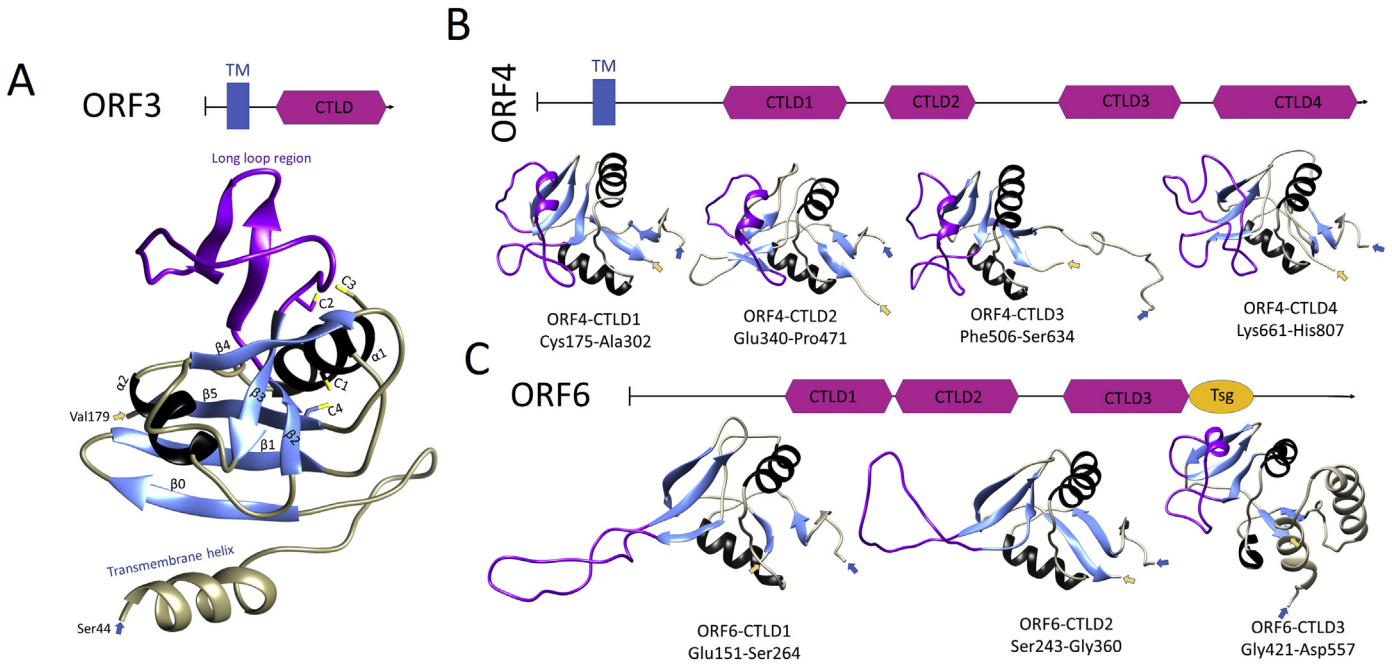

Fig. 6. Homology models investigating the possible structure of the C-type lectin-like domain containing proteins (CTLDcps) expressed by three novel genes located in the right end region of the bearded dragon adenovirus 1 genome. Canonical secondary structure elements of the C-type lectin-like domain (CTLD) fold are shown in blue if β-strand and in black if α-helix. The purple ribbon indicates the second loop of the fold of variable structure and length. The N-terminus is indicated by the blue, the C-terminus by the yellow arrows. Panel A shows the homology model of the entire ORF3 protein sequence, with the exception of the first 43 N-terminal residues. Panel B presents homology models of each CTLD detected in ORF4 and 6, respectively. (For interpretation of the references to colour in this figure legend, the reader is referred to the web version of this article.)

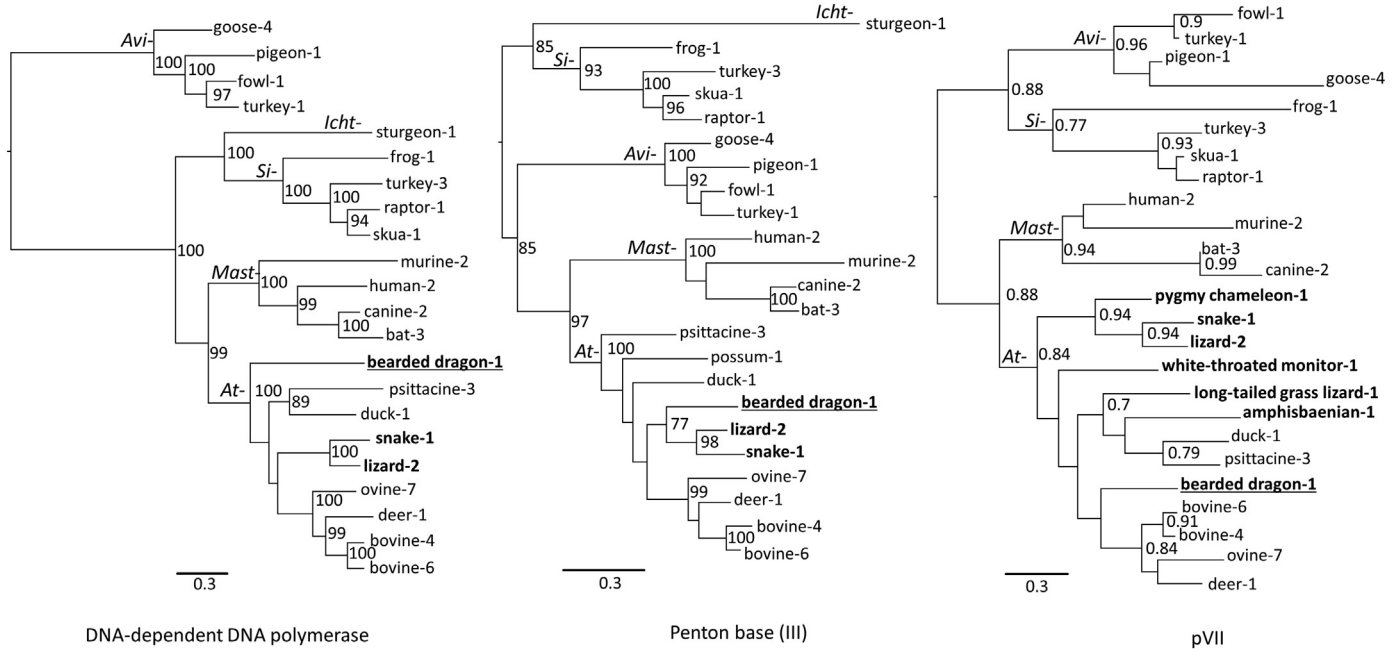

Fig. 7. Maximum likelihood phylogenetic calculations based on the complete protein sequence of three adenoviral proteins. All corresponding available sequences from genus *Atadeovirus* (*At-*) are represented. Members of four different species from the other genera, namely *Mastadenovirus* (*Mast-*), *Aviadenovirus* (*Avi-*), *Siadenovirus* (*Si-*) and *Ichtadenovirus* (*Icht-*) are also incorporated, where available. The DNA-dependent DNA polymerase (1070 aa in alignment) is a non-structural protein, whereas the penton (440 aa) is an immunogenic structural protein. The nucleoprotein pVII (124 aa) is a small non-immunogenic structural DNA-binding protein, available from most of the reptilian atadenoviruses described to date. Due to its varied conservation and short length, the reliability of the pVII calculations topology was tested by aLRT- Shimodaira-Hasegawa-like test, shown as node values. Topology reliability was tested by bootstrap of 1000 replicates in case of the other two inference. Percentage values derived from this are presented as node values if significant. Reptilian atadenoviruses are indicated in bold, sequences from bearded dragon adenovirus 1 are underlined.

possibility, that BDAdV-1 is a facultative pathogen of chronically-infected individuals is more likely. Interestingly, BDAdV-1 DNA was detected in the brain tissue of juvenile individuals with a history of CNS signs, suggesting that the pathogenicity, virulence of BDAdV-1 and the prognosis of such an infection might depend on the age of the affected animal.

As far as the coding region of the BDAdV-1 genome is concerned, its left end region displayed the typical *Atadenovirus*-like organization. This includes the presence of the genus-specific p32K and all three LH genes (Hess et al., 1997; Vrati et al., 1996; Farkas et al., 2008; Pénzes et al., 2014; To et al., 2014; Miller et al., 2017). The E1B 55 K is a non-structural early protein of mastadenoviruses, responsible for the degradation of cellular proteins so that a suitable environment for AdV replication can be established (Wienzek et al., 2000; Baker et al., 2007). LH3, however, its homologue in the *Atadenovirus*, has been shown to be structural and incorporated into the virion structure of ovine adenovirus 7 (OAdV-7), SnAdV-1 and LAdV-2 (Gorman et al., 2005; Pénzes et al., 2014; Menendez-Conejero et al., 2017). Still, LH3 seems to also fulfil the role in the degradation of cellular proteins (coupled to the E4.3 and E4.2 /34 K/ proteins, just as in the mastadenoviruses) (Gilson et al., 2016). The LH3 aa sequence displays high rate of conservation throughout the genus; 40 to 70% of the residues are identical between any two members. The BDAdV-1 LH3 displays a significantly lower rate of conservation, especially when considering the residues responsible for interacting with the neighbouring hexon towers. The sidechain charge of the polar residues differs significantly, which might imply that the BDAdV-1 capsid structure incorporates the LH3 trimers via interactions of a different nature than that of SnAdV-1. It remains to be determined by structural studies how these interactions manifest and whether they affect the biophysical characteristics of the BDAdV-1 capsid. Interestingly, BDAdV-1 also appears to harbour a divergent fiber knob, which, in concordance with our LH3 predictions, might suggest that the BDAdV-1 virions target different cellular receptors or glycans for entry compared to the SnAdV-1 fiber.

The splicing pattern of the adenoviral mRNA is considered to be characteristic in each genus, showing genus-level conservation (Davison et al., 2003). Interestingly, genus *Atadenovirus* displays a variety in the presence or absence of *Mastadenovirus*-like splicing features. Experimental evidence failed to predict splicing in the pol and IVa2-encoding mRNAs of OAdV-7 (Khatri and Both, 1998). Similarly, no such features could be predicted in the DAdV-1, SnAdV-1, PsAdV-3 or in the OdAdV-1 genomes, either (Hess et al., 1997; Farkas et al., 2008; To et al., 2014; Miller et al., 2017). LAdV-2, however, appears to harbour a spliced IVa2 (Pénzes et al., 2014) and our results suggest BDAdV-1 to express its pol using a spliced mRNA transcript.

The BDAdV-1 genome possesses a distinct right end region from any hitherto studied AdVs. The presence of its three E4 and the RH gene homologues, nevertheless, clearly indicates its affiliation with genus *Atadenovirus* (Gilson et al., 2016). Unlike atadenoviruses of squamate reptiles, which harbour only one RH gene homologue, ruminant and avian atadenoviruses possess multiple RH homologues, each of which has been shown to contain an N-terminal F-box domain (Both, 2002). Interestingly, this domain is missing from the SnAdV-1 RH, yet present in the LAdV-2 RH (Farkas et al., 2008; Pénzes et al., 2014). Proteins containing F-box domains are extremely abundant in metazoans and are parts of the Skp1-cullin-F-box (SCF) E3-ubiquitin ligase complex, which is responsible for marking cell cycle regulatory proteins for proteasomal degradation (Skowyra et al., 1997). The SCF E3-ubiquitin complex of atadenoviruses has been shown to include E4.3 and E4.2 as well, both encoded in close proximity on the *l* strand (Gilson et al., 2016). Our results suggest that gene duplication is a less common event in squamate atadenoviruses. The RH gene of BDAdV-1 is approximately twice as long as the average ruminant atadenovirus RH gene, which implies that BDAdV-1 may follow a different strategy of incorporating multiple F-box domains into a single long RH, in contrast with gene duplication.

The most unexpected feature of the BDAdV-1 genome was the presence of five right-end-located ORFs, which disclosed no detectable homology to any adenoviral ORFs to date. Three of these have the capability to encode proteins of the CTLD superfamily. According to the homology model, ORF3 shares a domain architecture with group II/V CTLDcps, similarly to all viral CTLDcps described so far, including ORF19 of genus *Aviadenovirus* (Ensser et al., 1997; Wilcock et al., 1999; Afonso et al., 2000; Galindo et al., 2000; Mullen et al., 2002; Chiocca et al., 1996). ORF3, however, displays protein sequence similarity only with a 23-aa-long segment at the predicted CTLD fold of ORF19, suggesting that these two adenoviral lineages obtained their II/V CTLDcps independently. UL45, an 18-kDa-sized CTLD group II late envelope protein of alphaherpesviruses, such as herpes simplex virus 1 (HSV-1) and equine herpesvirus 1, has been shown to be a virulence factor of minor to no role during in vitro replication (Oettler et al., 2001; Visalli and Brandt, 2002; Wyrwicz et al., 2008). Deletion of the HSV-1 UL45, however, resulted in a reduced ability of the HSV-1 virions to infect the CNS in a dose-dependent manor in vivo (Visalli and Brandt, 2002). Considering the presence of BDAdV-1 DNA in the brains of three juvenile bearded dragons with a history of CNS signs, the function of ORF3 might be associated with viral neurotropism.

Unlike ORF3, ORF4 and ORF6 harbour multiple CTLDs and both are unusually large compared to the other, typically short, ORFs of the corresponding AdV genome regions. Despite of the aa sequence similarity they display with cellular multidomain CTLDcps, their predicted domain architecture is considerably different. With the exception of group II/V CTLDcps, all membrane-bound members of the superfamily harbour an N-terminal extracellular and a short C-terminal cytoplasmatic domain, positioning the TM domain close to the C-terminus (Zelensky and Gready, 2005). Despite of the multiple consecutive macrophage mannose receptor-like CTLDs present in ORF4, these are located C-terminally from the TM, giving the protein opposite polarity from that of group VI CTLDcps. It is unknown whether ORF4 is incorporated into the BDAdV-1 capsid structure, nonetheless the prospect of it being structural, which is implied by its position on the *r* strand, and mimic a macrophage mannose receptor-like CTLDcp is an intriguing one. The *l*-strand-encoded ORF6, in contrast, lacks the TM domain. Its predicted domain architecture, however, indicates no resemblance to any of the CTLDcp groups established thus far, including even the soluble ones. A large number of soluble CTLDcps play a crucial role in the process of phagocytosis by binding to carbohydrate patterns associated with pathogens (Kerrigan and Brown, 2009). As BDAdV-1 appears to cause a systematic infection in bearded dragons, it is a possibility that the deliberate phagocytotic uptake of virions by cellular host immune components plays a role in systematic spreading. When considering how the reptilian cellular immune response relies almost exclusively on the phagocytotic innate components rather than on the slow-reacting adaptive cellular immune process (Zimmerman et al., 2010) this explanation might be a plausible one.

In concordance with its divergent, albeit atadenovirus-like genome, phylogenetic inference indicated no close relationship between BDAdV-1 and other reptilian atadenoviruses. The only exception, however, appears to be the calculations based on the penton base. As the penton is an antigenic structural protein, its aa sequence has probably adapted to the host immune system, masking real evolutionary relationships among these AdVs. Alternatively, recombination could also explain this phenomenon, even though the BDAdV-1 penton protein sequence is equally 74% identical to both currently-determined squamate atadenovirus penton bases of SnAdV-1 and LadV-2. The recent detection of LAdV-2 DNA from captive inland bearded dragons (Benge et al., 2019) indicates that *P. vitticeps* possibly serves as a host to multiple atadenovirus types besides BDAdV-1, which could have provided a situation suitable for such events to take place. As genus *Atadenovirus* has been concluded to be of squamate reptile origin (Harrach et al., 1997; Wellehan et al., 2004; Farkas et al., 2008; Harrach et al., 2011), the paraphyly of reptilian atadenoviruses, as displayed by the pol- and pVII-

based inference, is to be expected, especially with the respective monophyly of avian and ruminant members of the genus. To resolve the exact order of host witch events to birds and ruminants, however, would require the analysis of further complete reptilian atadenoviral genomes. Unfortunately, in case of the pVII calculation, we must not dismiss the stochasticity originating from the fact that this protein includes highly conserved positively-charged residues due to its DNA-binding nature while it is short in length.

Taken together, the complete genome sequence of BDAdV-1 sheds new light on both AdV diversity and on the evolution of genus *Atadenovirus*. At the same time, the analysis of its divergent genome provided unforeseen characteristics, with a capability to explain aspects of its observed pathogenesis. Moreover, it presents the possibility of investigating the structure and function of novel proteins from an abundant, albeit relatively well-characterized group of proteins, such as the CTLD superfamily. Even if its genome sequence was not determined from a cell culture isolate, BDAdV-1 can still be classified into a new species within genus *Atadenovirus* of *Adenoviridae*, under the potential name of Lizard atadenovirus B (Simmonds et al., 2017).

Funding information

This work was supported partly by a grant provided by the Hungarian Scientific Research Fund (OTKA NN128309).

Conflicts of interest

The authors declare that there are no conflicts of interest

Ethical statement

None of the experiments performed during this study involved living animals. We hereby certify that all experiments were carried out in conformation with the Federation of European Laboratory Animal Science Associations (FELASA) guidelines and recommendations on deceased vertebrates. The deceased animals involved in the experiments were processed in an institution dedicated to veterinary medical science. All corpses originated from individuals, which were bred and kept in captivity and none of the samples originated from a species listed under the Convention on International Trade in Endangered Species (CITES).

Appendix A. Supplementary data

Supplementary data to this article can be found online at https://doi.org/10.1016/j.meegid.2020.104321.

References

Abbas, M.D., Marschang, R.E., Schmidt, V., Kasper, A., Papp, T., 2011. A unique novel reptilian paramyxovirus, four atadenovirus types and a reovirus identified in a concurrent infection of a corn snake (*Pantherophis guttatus*) collection in Germany. Vet. Microbiol. 150 (1–2), 70–79. https://doi.org/10.1016/j.vetmic.2011.01.010.

Afonso, C.L., Tulman, E.R., Lu, Z., Zsak, L., Kutish, G.F., Rock, D.L., 2000. The genome of fowlpox virus. J. Virol. 74 (8), 3815–3831. https://doi.org/10.1128/jvi.74.8.3815-3831.2000.

Almagro Armenteros, J.J., Tsirigos, K.D., Sonderby, C.K., Petersen, T.N., Winther, O., Brunak, S., von Heijne, G., Nielsen, H., 2019. SignalP 5.0 improves signal peptide predictions using deep neural networks. Nat. Biotechnol. 37 (4), 420–423. https://doi.org/10.1038/s41587-019-0036-z.

Baker, A., Rohleder, K.J., Hanakahi, L.A., Ketner, G., 2007. Adenovirus E4 34k and E1b 55k oncoproteins target host DNA ligase IV for proteasomal degradation. J. Virol. 81 (13), 7034–7040. https://doi.org/10.1128/jvi.00029-07.

Ball, I., Behncke, H., Schmidt, V., Geflugel, F.T., Papp, T., Stohr, A.C., Marschang, R.E., 2014. Partial characterization of new adenoviruses found in lizards. J. Zool, Wildl. Med. 45 (2), 287–297. https://doi.org/10.1638/2013-0143.1.

Benge, S.L., Hyndman, T.H., Funk, R.S., Marschang, R.E., Schneider, R., Childress, A.L., Wellehan Jr., J.F.X., 2019. Identification of helodermatid adenovirus 2 in a captive central bearded dragon (Pogona vitticeps), wild gila monsters (Heloderma suspectum), and a death adder (acanthophis antarcticus). J. Zool. Wildl. Med. 50 (1), 238–242. https://doi.org/10.1638/2017-0016.

Benkő, M., Elo, P., Ursu, K., Ahne, W., LaPatra, S.E., Thomson, D., Harrach, B., 2002. First molecular evidence for the existence of distinct fish and snake adenoviruses. J. Virol. 76 (19), 10056–10059. https://doi.org/10.1128/jvi.76.19.10056-10059.2002.

Both, G.W., 2002. Identification of a unique family of F-box proteins in atadenoviruses. Virology 304 (2), 425–433. https://doi.org/10.1006/viro.2002.1734.

Carver, T., Harris, S.R., Berriman, M., Parkhill, J., McQuillan, J.A., 2012. Artemis: an integrated platform for visualization and analysis of high-throughput sequence-based experimental data. Bioinformatics 28 (4), 464–469. https://doi.org/10.1093/bioinformatics/btr703.

Chiocca, S., Kurzbauer, R., Schaffner, G., Baker, A., Mautner, V., Cotten, M., 1996. The complete DNA sequence and genomic organization of the avian adenovirus CELO. J. Virol. 70 (5), 2939–2949.

Dan, A., Elo, P., Harrach, B., Zadori, Z., Benkő, M., 2001. Four new inverted terminal repeat sequences from bovine adenoviruses reveal striking differences in the length and content of the ITRs. Virus Genes 22 (2), 175–179. https://doi.org/10.1023/a:1008125324346.

Darriba, D., Taboada, G.L., Doallo, R., Posada, D., 2011. ProtTest 3: fast selection of best-fit models of protein evolution. Bioinformatics 27 (8), 1164–1165. https://doi.org/10.1093/bioinformatics/btr088.

Davison, A.J., Wright, K.M., Harrach, B., 2000. DNA sequence of frog adenovirus. J. Gen. Virol. 81 (Pt 10), 2431–2439. https://doi.org/10.1099/0022-1317-81-10-2431.

Davison, A.J., Benkő, M., Harrach, B., 2003. Genetic content and evolution of adenoviruses. J. Gen. Virol. 84 (Pt 11), 2895–2908. https://doi.org/10.1099/vir.0.19497-0.

de Oliveira, A.P.J., Rangel, M.C.V., Vidovszky, M.Z., Rossi, J.L., Vicentini, F., Harrach, B., Kaján, G.L., 2020. Identification of two novel adenoviruses in smooth-billed ani and tropical screech owl. PLoS One 10 (2), e0229415. https://doi.org/10.1371/journal.pone.0229415.

Doneley, R.J., Buckle, K.N., Hulse, L., 2014. Adenoviral infection in a collection of juvenile inland bearded dragons (*Pogona vitticeps*). Aust. Vet. J. 92 (1–2), 41–45. https://doi.org/10.1111/avj.12136.

Doszpoly, A., Harrach, B., LaPatra, S., Benkő, M., 2019. Unconventional gene arrangement and content revealed by full genome analysis of the white sturgeon adenovirus, the single member of the genus *Ichtadenovirus*. Infect. Genet. Evol. 75, 103976. https://doi.org/10.1016/j.meegid.2019.103976.

Duarte, M.A., Silva, J.M.F., R. Brito C, S. Teixeira D, L. Melo F, M. Ribeiro B, T. Nagata, and S. Campos F., 2019. Faecal Virome analysis of wild animals from Brazil. Viruses 11 (9), E803. https://doi.org/10.3390/v11090803.

Ensser, A., Pflanz, R., Fleckenstein, B., 1997. Primary structure of the alcelaphine herpesvirus 1 genome. J. Virol. 71 (9), 6517–6525.

Farkas, S.L., Harrach, B., Benkő, M., 2008. Completion of the genome analysis of snake adenovirus type 1, a representative of the reptilian lineage within the novel genus Atadenovirus. Virus Res. 132 (1–2), 132–139. https://doi.org/10.1016/j.virusres.2007.11.009.

Felsenstein, J. 1993. PHYLIP (phylOgeny Inference Package) version 3.5c. Distributed by the Author.

Fox, K.A., Atwater, L., Hoon-Hanks, L., Miller, M., 2017. A mortality event in elk (*Cervus elaphus nelsoni*) calves associated with malnutrition, pasteurellosis, and deer adenovirus in Colorado, USA. J. Wildl. Dis. 53 (3), 674–676. https://doi.org/10.7589/2016-07-167.

Fredholm, D.V., Coleman, J.K., Childress, A.L., Wellehan Jr., J.F., 2015. Development and validation of a novel hydrolysis probe real-time polymerase chain reaction for agamid adenovirus 1 in the central bearded dragon (Pogona vitticeps). J. Vet. Diagn. Investig. 27 (2), 249–253. https://doi.org/10.1177/1040638715576564.

Gal, J., Mandoki, M., Sos, E., Kertesz, P., Koroknai, V., Banyai, K., Farkas, S.L., 2017. Novel adenovirus detected in kowari (Dasyuroides byrnei) with pneumonia. Acta Microbiol. Immunol. Hung. 64 (1), 81–90. https://doi.org/10.1556/030.63.2016.024.

Galindo, I., Almazan, F., Bustos, M.J., Vinuela, E., Carrascosa, A.L., 2000. African swine fever virus EP153R open reading frame encodes a glycoprotein involved in the hemadsorption of infected cells. Virology 266 (2), 340–351. https://doi.org/10.1006/viro.1999.0080.

Garcia-Morante, B., Pénzes, J.J., Costa, T., Martorell, J., Martinez, J., 2016. Hyperplastic stomatitis and esophagitis in a tortoise (Testudo graeca) associated with an adenovirus infection. J. Vet. Diagn. Investig. 28 (5), 579–583. https://doi.org/10.1177/1040638716659903.

Gilson, T., Blanchette, P., Ballmann, M.Z., Papp, T., Pénzes, J.J., Benkő, M., Harrach, B., Branton, P.E., 2016. Using the E4orf6-based E3 ubiquitin ligase as a tool to analyze the evolution of adenoviruses. J. Virol. 90 (16), 7350–7367. https://doi.org/10.1128/jvi.00420-16.

Gorman, J.J., Wallis, T.P., Whelan, D.A., Shaw, J., Both, G.W., 2005. LH3, a "homologue" of the mastadenoviral E1B 55-kDa protein is a structural protein of atadenoviruses. Virology 342 (1), 159–166. https://doi.org/10.1016/j.virol.2005.07.020.

Guindon, S., Dufayard, J.F., Lefort, V., Anisimova, M., Hordijk, W., Gascuel, O., 2010. New algorithms and methods to estimate maximum-likelihood phylogenies: assessing the performance of PhyML 3.0. Syst. Biol. 59 (3), 307–321. https://doi.org/10.1093/sysbio/syq010.

Harrach, B., Meehan, B.M., Benkő, M., Adair, B.M., Todd, D., 1997. Close phylogenetic relationship between egg drop syndrome virus, bovine adenovirus serotype 7, and ovine adenovirus strain 287. Virology 229 (1), 302–308. https://doi.org/10.1006/viro.1996.8390.

Harrach, B., Benkő, M., Both, G.W., Brown, M., Davison, A.J., Echavarría, M., Hess, M., Jones, M.S., Kajon, A., Lehmkuhl, H.D., Mautner, V., Mittal, S.K., Wadell, G., 2011. Family *Adenoviridae*. In: King, A.M.Q., Adams, M.J., Carstens, E.B., Lefkowitz, Elliot J. (Eds.), Virus Taxonomy: Classification and Nomenclature of Viruses: Ninth Report of the International Committee on the Taxonomy of Viruses. Elsevier, San

Francisco,CA, USA, pp. 125–141. https://talk.ictvonline.org/ictv-reports/ictv_9th_report/dsdna-viruses-2011/w/dsdna_viruses/93/adenoviridae.
Harrach, B., Tarjan, Z.L., Benkő, M., 2019. Adenoviruses across the animal kingdom: a walk in the zoo. FEBS Lett. 593 (24), 3660–3673. https://doi.org/10.1002/1873-3468.13687.
Hess, M., Blocker, H., Brandt, P., 1997. The complete nucleotide sequence of the egg drop syndrome virus: an intermediate between mastadenoviruses and aviadenoviruses. Virology 238 (1), 145–156. https://doi.org/10.1006/viro.1997.8815.
Hyndman, T., Shilton, C.M., 2011. Molecular detection of two adenoviruses associated with disease in Australian lizards. Aust. Vet. J. 89 (6), 232–235. https://doi.org/10.1111/j.1751-0813.2011.00712.x.
Hyndman, T.H., Howard, J.G., Doneley, R.J., 2019. Adenoviruses in free-ranging Australian bearded dragons (Pogona spp.). Vet. Microbiol. 234, 72–76. https://doi.org/10.1016/j.vetmic.2019.05.014.
Kaján, G.L., Davison, A.J., Palya, V., Harrach, B., Benkő, M., 2012. Genome sequence of a waterfowl aviadenovirus, goose adenovirus 4. J. Gen. Virol. 93 (Pt 11), 2457–2465. https://doi.org/10.1099/vir.0.042028-0.
Kerrigan, A.M., Brown, G.D., 2009. C-type lectins and phagocytosis. Immunobiology 214 (7), 562–575. https://doi.org/10.1016/j.imbio.2008.11.003.
Khatri, A., Both, G.W., 1998. Identification of transcripts and promoter regions of ovine adenovirus OAV287. Virology 245 (1), 128–141. https://doi.org/10.1006/viro.1998.9136.
Kovács, E.R., Benkő, M., 2011. Complete sequence of raptor adenovirus 1 confirms the characteristic genome organization of siadenoviruses. Infect. Genet. Evol. 11 (5), 1058–1065. https://doi.org/10.1016/j.meegid.2011.03.021.
Krogh, A., Larsson, B., von Heijne, G., Sonnhammer, E.L., 2001. Predicting transmembrane protein topology with a hidden Markov model: application to complete genomes. J. Mol. Biol. 305 (3), 567–580. https://doi.org/10.1006/jmbi.2000.4315.
Kübber-Heiss, A., Benetka, V., Filip, T., Benyr, G., Schilcher, F., Pallan, C., Möstl, K., 2006. First detection of an adenovirus infection in a bearded dragon (*Pogona vitticeps)* in Austria. Wiener Tierarztliche Monatsschrift 93 (3), 68–72.
Kubiak, M., 2013. Detection of agamid Adenovirus-1 in clinically healthy bearded dragons (Pogona vitticeps) in the UK. Vet. Rec. 172 (18), 475. https://doi.org/10.1136/vr.101087.
Letunic, I., Bork, P., 2018. 20 years of the SMART protein domain annotation resource. Nucleic Acids Res. 46 (D1), D493–d496. https://doi.org/10.1093/nar/gkx922.
Lobley, A., Sadowski, M.I., Jones, D.T., 2009. pGenTHREADER and pDomTHREADER: new methods for improved protein fold recognition and superfamily discrimination. Bioinformatics 25 (14), 1761–1767. https://doi.org/10.1093/bioinformatics/btp302.
Menendez-Conejero, R., Nguyen, T.H., Singh, A.K., Condezo, G.N., Marschang, R.E., van Raaij, M.J., San Martin, C., 2017. Structure of a reptilian adenovirus reveals a phage Tailspike fold stabilizing a vertebrate virus capsid. Structure 25 (10). https://doi.org/10.1016/j.str.2017.08.007. 1562-1573.e5.
Middleton, D., Curran, M., Maxwell, L., 2002. Natural killer cells and their receptors. Transpl. Immunol. 10 (2–3), 147–164. https://doi.org/10.1016/s0966-3274(02)00062-x.
Miller, M.M., Cornish, T.E., Creekmore, T.E., Fox, K., Laegreid, W., McKenna, J., Vasquez, M., Woods, L.W., 2017. Whole-genome sequences of Odocoileus hemionus deer adenovirus isolates from deer, moose and elk are highly conserved and support a new species in the genus *Atadenovirus*. J. Gen. Virol. 98 (9), 2320–2328. https://doi.org/10.1099/jgv.0.000880.
Mullen, M.M., Haan, K.M., Longnecker, R., Jardetzky, T.S., 2002. Structure of the Epstein-Barr virus gp42 protein bound to the MHC class II receptor HLA-DR1. Mol. Cell 9 (2), 375–385. https://doi.org/10.1016/s1097-2765(02)00465-3.
Needle, D.B., Wise, A.G., Gregory, C.R., Maes, R.K., Sidor, I.F., Ritchie, B.W., Agnew, D., 2019. Necrotizing ventriculitis in fledgling chimney swifts (Chaetura Pelagica) associated with a novel adenovirus, chimney swift Adenovirus-1 (CsAdV-1). Vet. Pathol. 56 (6), 907–914. https://doi.org/10.1177/0300985819861717.
Nguyen, T.H., Vidovszky, M.Z., Ballmann, M.Z., Sanz-Gaitero, M., Singh, A.K., Harrach, B., Benkő, M., van Raaij, M.J., 2015. Crystal structure of the fibre head domain of bovine adenovirus 4, a ruminant atadenovirus. Virol. J. 12, 81. https://doi.org/10.1186/s12985-015-0309-1.
Oettler, D., Kaaden, O.R., Neubauer, A., 2001. The equine herpesvirus 1 UL45 homolog encodes a glycosylated type II transmembrane protein and is involved in virus egress. Virology 279 (1), 302–312. https://doi.org/10.1006/viro.2000.0690.
Okonechnikov, K., Golosova, O., Fursov, M., 2012. Unipro UGENE: a unified bioinformatics toolkit. Bioinformatics 28 (8), 1166–1167. https://doi.org/10.1093/bioinformatics/bts091.
Papp, T., Fledelius, B., Schmidt, V., Kaján, G.L., Marschang, R.E., 2009. PCR-sequence characterization of new adenoviruses found in reptiles and the first successful isolation of a lizard adenovirus. Vet. Microbiol. 134 (3–4), 233–240. https://doi.org/10.1016/j.vetmic.2008.08.003.
Park, Y.M., Kim, J.H., Gu, S.H., Lee, S.Y., Lee, M.G., Kang, Y.K., Kang, S.H., Kim, H.J., Song, J.W., 2012. Full genome analysis of a novel adenovirus from the south polar skua (Catharacta maccormicki) in Antarctica. Virology 422 (1), 144–150. https://doi.org/10.1016/j.virol.2011.10.008.
Parkin, D.B., Archer, L.L., Childress, A.L., Wellehan Jr., J.F., 2009. Genotype differentiation of agamid adenovirus 1 in bearded dragons (Pogona vitticeps) in the USA by hexon gene sequence. Infect. Genet. Evol. 9 (4), 501–506. https://doi.org/10.1016/j.meegid.2009.01.010.
Pénzes, J.J., Menendez-Conejero, R., Condezo, G.N., Ball, I., Papp, T., Doszpoly, A., Paradela, A., Perez-Berna, A.J., Lopez-Sanz, M., Nguyen, T.H., van Raaij, M.J., Marschang, R.E., Harrach, B., Benkő, M., San Martin, C., 2014. Molecular characterization of a lizard adenovirus reveals the first atadenovirus with two fiber genes and the first adenovirus with either one short or three long fibers per penton. J. Virol. 88 (19), 11304–11314. https://doi.org/10.1128/jvi.00306-14.
Pettersen, E.F., Goddard, T.D., Huang, C.C., Couch, G.S., Greenblatt, D.M., Meng, E.C., Ferrin, T.E., 2004. UCSF chimera–a visualization system for exploratory research and analysis. J. Comput. Chem. 25 (13), 1605–1612. https://doi.org/10.1002/jcc.20084.
Phalen, D.N., Agius, J., Vaz, F.F., Eden, J.S., Setyo, L.C., Donahoe, S., 2019. A survey of a mixed species aviary provides new insights into the pathogenicity, diversity, evolution, host range, and distribution of psittacine and passerine adenoviruses. Avian Pathol. 48 (5), 437–443. https://doi.org/10.1080/03079457.2019.1617835.
Prado-Irwin, S.R., van de Schoot, M., Geneva, A.J., 2018. Detection and phylogenetic analysis of adenoviruses occurring in a single anole species. PeerJ 6, e5521. https://doi.org/10.7717/peerj.5521.
Reese, M.G., Eeckman, F.H., Kulp, D., Haussler, D., 1997. Improved splice site detection in genie. J. Comput. Biol. 4 (3), 311–323. https://doi.org/10.1089/cmb.1997.4.311.
Schilliger, L., Mentre, V., Marschang, R.E., Nicolier, A., Richter, B., 2016. Triple infection with agamid adenovirus 1, Encephaliton cuniculi-like microsporidium and enteric coccidia in a bearded dragon (Pogona vitticeps). Tierarztl Prax Ausg K Kleintiere Heimtiere 44 (5), 355–358. https://doi.org/10.15654/tpk-150790.
Simmonds, P., Adams, M.J., Benkő, M., Breitbart, M., Brister, J.R., Carstens, E.B., Davison, A.J., Delwart, E., Gorbalenya, A.E., Harrach, B., Hull, R., King, A.M., Koonin, E.V., Krupovic, M., Kuhn, J.H., Lefkowitz, E.J., Nibert, M.L., Orton, R., Roossinck, M.J., Sabanadzovic, S., Sullivan, M.B., Suttle, C.A., Tesh, R.B., van der Vlugt, R.A., Varsani, A., Zerbini, F.M., 2017. Consensus statement: virus taxonomy in the age of metagenomics. Nat. Rev. Microbiol. 15 (3), 161–168. https://doi.org/10.1038/nrmicro.2016.177.
Singh, A.K., Menendez-Conejero, R., San Martin, C., van Raaij, M.J., 2014. Crystal structure of the fibre head domain of the Atadenovirus Snake adenovirus 1. PLoS One 9 (12), e114373. https://doi.org/10.1371/journal.pone.0114373.
Skowyra, D., Craig, K.L., Tyers, M., Elledge, S.J., Harper, J.W., 1997. F-box proteins are receptors that recruit phosphorylated substrates to the SCF ubiquitin-ligase complex. Cell 91 (2), 209–219. https://doi.org/10.1016/s0092-8674(00)80403-1.
Staden, R., Beal, K.F., Bonfield, J.K., 2000. The Staden package, 1998. Methods Mol. Biol. 132, 115–130. https://doi.org/10.1385/1-59259-192-2:115.
Stockert, R.J., 1995. The asialoglycoprotein receptor: relationships between structure, function, and expression. Physiol. Rev. 75 (3), 591–609. https://doi.org/10.1152/physrev.1995.75.3.591.
Suchard, M.A., Lemey, P., Baele, G., Ayres, D.L., Drummond, A.J., Rambaut, A., 2018. Bayesian phylogenetic and phylodynamic data integration using BEAST 1.10. Virus Evol. 4 (1). https://doi.org/10.1093/ve/vey016. vey016.
Szirovicza, L., Lopez, P., Kopena, R., Benkő, M., Martin, J., Pénzes, J.J., 2016. Random sampling of squamate reptiles in Spanish natural reserves reveals the presence of novel adenoviruses in Lacertids (family Lacertidae) and worm lizards (Amphisbaenia). PLoS One 11 (7), e0159016. https://doi.org/10.1371/journal.pone.0159016.
Thomson, D., Meers, J., Harrach, B., 2002. Molecular confirmation of an adenovirus in brushtail possums (Trichosurus vulpecula). Virus Res. 83 (1–2), 189–195. https://doi.org/10.1016/s0168-1702(01)00437-3.
Tischer, S., Geyeregger, R., Kwoczek, J., Heim, A., Figueiredo, C., Blasczyk, R., Maecker-Kolhoff, B., Eiz-Vesper, B., 2016. Discovery of immunodominant T-cell epitopes reveals penton protein as a second immunodominant target in human adenovirus infection. J. Transl. Med. 14 (1), 286. https://doi.org/10.1186/s12967-016-1042-2.
To, K.K., Tse, H., Chan, W.M., Choi, G.K., Zhang, A.J., Sridhar, S., Wong, S.C., Chan, J.F., Chan, A.S., Woo, P.C., Lau, S.K., Lo, J.Y., Chan, K.H., Cheng, V.C., Yuen, K.Y., 2014. A novel psittacine adenovirus identified during an outbreak of avian chlamydiosis and human psittacosis: zoonosis associated with virus-bacterium coinfection in birds. PLoS Negl. Trop. Dis. 8 (12), e3318. https://doi.org/10.1371/journal.pntd.0003318.
Vidovszky, M.Z., Szeredi, L., Doszpoly, A., Harrach, B., Hornyak, A., 2019. Isolation and complete genome sequence analysis of a novel ovine adenovirus type representing a possible new mastadenovirus species. Arch. Virol. 164 (8), 2205–2207. https://doi.org/10.1007/s00705-019-04299-6.
Visalli, R.J., Brandt, C.R., 2002. Mutation of the herpes simplex virus 1 KOS UL45 gene reveals dose dependent effects on central nervous system growth. Arch. Virol. 147 (3), 519–532. https://doi.org/10.1007/s007050200004.
Vrati, S., Brookes, D.E., Strike, P., Khatri, A., Boyle, D.B., Both, G.W., 1996. Unique genome arrangement of an ovine adenovirus: identification of new proteins and proteinase cleavage sites. Virology 220 (1), 186–199. https://doi.org/10.1006/viro.1996.0299.
Wallace, I.M., O'Sullivan, O., Higgins, D.G., Notredame, C., 2006. M-coffee: combining multiple sequence alignment methods with T-coffee. Nucleic Acids Res. 34 (6), 1692–1699. https://doi.org/10.1093/nar/gkl091.
Waterhouse, A., Bertoni, M., Bienert, S., Studer, G., Tauriello, G., Gumienny, R., Heer, F.T., de Beer, T.A.P., Rempfer, C., Bordoli, L., Lepore, R., Schwede, T., 2018. SWISS-MODEL: homology modelling of protein structures and complexes. Nucleic Acids Res. 46 (W1), W296–w303. https://doi.org/10.1093/nar/gky427.
Webb, B., Sali, A., 2016. Comparative protein structure modeling using MODELLER. Curr. Protoc. Protein Sci. 86, 2.9.1–2.9.37. https://doi.org/10.1002/cpps.20.
Wellehan, J.F., Johnson, A.J., Harrach, B., Benkő, M., Pessier, A.P., Johnson, C.M., Garner, M.M., Childress, A., Jacobson, E.R., 2004. Detection and analysis of six lizard adenoviruses by consensus primer PCR provides further evidence of a reptilian origin for the atadenoviruses. J. Virol. 78 (23), 13366–13369. https://doi.org/10.1128/jvi.78.23.13366-13369.2004.
Wienzek, S., Roth, J., Dobbelstein, M., 2000. E1B 55-kilodalton oncoproteins of adenovirus types 5 and 12 inactivate and relocalize p53, but not p51 or p73, and cooperate with E4orf6 proteins to destabilize p53. J. Virol. 74 (1), 193–202. https://doi.org/10.1128/jvi.74.1.193-202.2000.
Wilcock, D., Duncan, S.A., Traktman, P., Zhang, W.H., Smith, G.L., 1999. The vaccinia virus A4OR gene product is a nonstructural, type II membrane glycoprotein that is

expressed at the cell surface. J. Gen. Virol. 80 (Pt 8), 2137–2148. https://doi.org/10.1099/0022-1317-80-8-2137.
Wyrwicz, L.S., Ginalski, K., Rychlewski, L., 2008. HSV-1 UL45 encodes a carbohydrate binding C-type lectin protein. In: Cell Cycle, pp. 269–271 United States.
Zelensky, A.N., Gready, J.E., 2003. Comparative analysis of structural properties of the C-type-lectin-like domain (CTLD). Proteins 52 (3), 466–477. https://doi.org/10.1002/prot.10626.
Zelensky, A.N., Gready, J.E., 2005. The C-type lectin-like domain superfamily. FEBS J. 272 (24), 6179–6217. https://doi.org/10.1111/j.1742-4658.2005.05031.x.
Zhao, H., Chen, M., Pettersson, U., 2014. A new look at adenovirus splicing. Virology 456-457, 329–341. https://doi.org/10.1016/j.virol.2014.04.006.
Zimmerman, L.M., Vogel, L.A., Bowden, R.M., 2010. Understanding the vertebrate immune system: insights from the reptilian perspective. J. Exp. Biol. 213 (5), 661–671. https://doi.org/10.1242/jeb.038315.